Wind Energy Input to the Ekman Layer*

WEI WANG

Physical Oceanography Laboratory, Ocean University of China, Qingdao, Shandong, China

RUI XIN HUANG

Department of Physical Oceanography, Woods Hole Oceanographic Institution, Woods Hole, Massachusetts

ABSTRACT

Wind stress energy input through the surface ageostrophic currents is studied. The surface ageostrophic velocity is calculated using the classical formula of the Ekman spiral, with the Ekman depth determined from an empirical formula. The total amount of energy input over the global oceans for subinertial frequency is estimated as 2.4 TW averaged over a period from 1997 to 2002, or 2.3 TW averaged over a period from 1948 to 2002, based on daily wind stress data from NCEP–NCAR. Thus, in addition to the energy input to the near inertial waves of 0.5–0.7 TW reported by Alford and by Watanabe and Hibiya, the total energy input to the Ekman layer is estimated as 3 TW. This input is concentrated primarily over the Southern Ocean and the storm track in both the North Pacific and North Atlantic Oceans.

1. Introduction

To maintain the quasi-steady circulation in the ocean, a source of mechanical energy is required to balance the loss of mechanical energy from dissipation. Thus, the distribution of energy sources and sinks dictates the strength of circulation and its variability (Munk and Wunsch 1998; Huang 1998, 1999). This fundamental rule has been overlooked in the past. In fact, a common practice in the study of oceanic general circulation, either theoretically or numerically, has been based on certain arbitrary choices of vertical (diapycnal) mixing parameterization, without checking whether the external mechanical energy required to sustain such parameterization exists in the ocean.

Energetics of ocean circulation were discussed in pioneering works by Faller (1966) and Lueck and Reid (1984). However, many important terms of global energetics remain unknown. Faller (1966) estimated that wind stress contribution to local mixing is about 8 TW and to large-scale circulation is about 1 TW. Using a single sentence, Lueck and Reid (1984) stated that the total amount of energy input to the ocean by wind stress

is 2%–10% of the downward flux of energy (510 TW) in the atmospheric planetary boundary layer.

It is only within the past few years that the oceanography community has come to realize the vital importance of external sources of mechanical energy of the ocean circulation. The contribution from tidal dissipation is estimated at 0.9 TW for the deep ocean by Munk and Wunsch (1998). The contribution from wind stress to geostrophic current is estimated as 1.3 TW by Wunsch (1998). The contribution to gravitational potential energy (GPE hereinafter) from geothermal heating is small, about 0.05 TW (Huang 1999, 2002). The contribution from wind stress to the near-inertial motions in the upper ocean has been recently estimated at 0.5 TW (Alford 2003) or 0.7 TW (Watanaba and Hibiya 2002). (These authors disagree on details of the method; however, the slab models used in their studies are crude approximations for the complex processes in the ocean, and the difference in the energy estimate is too slight to be of concern.)

We recently extended the Sandstrom theorem (Sandstrom 1916) in two ways. First, we argue that convective adjustment induced by cooling (buoyancy loss) can lead to a substantial amount of GPE loss in the mixed layer, which is about 0.24 TW (Huang and Wang 2003, unpublished manuscript). Second, a large amount of GPE, estimated at 1.1 TW, is lost by conversion of eddy energy through baroclinic instability (Huang and Wang 2003, unpublished manuscript).

In addition, wind stress applies to the sea surface and

Corresponding author address: R. X. Huang, Department of Physical Oceanography, Woods Hole Oceanographic Institution, Woods Hole, MA 02543.
E-mail: rhuang@whoi.edu

drives both surface currents and waves. The mechanical energy input from the wind stress to the ocean is

$$W_{\text{wind}} = \boldsymbol{\tau} \cdot \mathbf{U}_0 + \overline{\boldsymbol{\tau}_1' \cdot \mathbf{u}_0'} + \overline{p' w_0'}, \quad (1)$$

where $\boldsymbol{\tau}$ and $\mathbf{U}_0$ are spatially averaged tangential stress and surface velocity for frequency much lower than the surface waves, $\boldsymbol{\tau}'$ and $\mathbf{u}_0'$ are high-frequency perturbations associated with surface waves, and p' and w_0' are perturbations of the surface pressure and velocity component normal to the surface. The second and third terms on the right-hand side of Eq. (1) represent wind stress work on the surface waves, which is discussed in a separate study by Wang and Huang (2004).

The first term on the right-hand side of Eq. (1) is the wind stress work on the quasi-steady currents on the surface, and quasi steadiness is defined in comparison with the time scale of typical surface waves. The surface velocity has two components:

$$\mathbf{U}_0 = \mathbf{U}_{0,G} + \mathbf{U}_{0,\text{AG}}, \quad (2)$$

that is, the geostrophic current and the ageostrophic current (surface Ekman transport). Wind stress energy input to the surface geostrophic currents has been discussed by Wunsch (1998), and so our study here is focused on the second term in Eq. (2).

2. Energetics of the Ekman layer

a. Energy balance

The horizontal momentum equations are

$$u_t - fv = (Au_z)_z \quad \text{and} \quad v_t + fu = (Av_z)_z, \quad (3)$$

with the boundary conditions

$$Au_z|_{z=0} = \tau^x/\rho_w \quad \text{and} \quad Av_z|_{z=0} = \tau^y/\rho_w;$$
$$u, v \rightarrow 0, \qquad \text{at } z \rightarrow -\infty, \quad (4)$$

where A is the vertical momentum diffusivity.

Multiplying these two equations by u and v and then integrating the result over the depth of the ocean, we obtain the energy balance

$$E_t = S - D, \quad (5)$$

where

$$E = \rho_w \int_{-\infty}^{0} 0.5(u^2 + v^2) \, dz,$$
$$S = \tau^x u(0) + \tau^y v(0), \quad \text{and}$$
$$D = \rho_w \int_{-\infty}^{0} A(u_z^2 + v_z^2) \, dz \quad (6)$$

are the total kinetic energy of the Ekman layer, the rate of wind energy input, and the dissipation rate, respectively. Note that 1) for a steady problem, the rate of dissipation is equal to the rate of wind stress energy input:

$$\tau^x u(0) + \tau^y v(0) = \rho_w \int_{-\infty}^{0} A(u_z^2 + v_z^2) \, dz, \quad (7)$$

and 2) the energy sink in the Ekman spiral is fed to the turbulence and internal waves and thus sustains the mixing in the Ekman layer and the mixed layer in the ocean.

The general solution including the geostrophic flow can be derived as follows. The horizontal momentum equations are

$$u_t^* - fv^* = -p_{s,x}/\rho_w + (Au_z^*)_z \quad \text{and}$$
$$v_t^* + fu^* = -p_{s,y}/\rho_w + (Av_z^*)_z, \quad (8)$$

where $u^* = u_g + u_e$ and $v^* = v_g + v_e$ are the sum of geostrophic velocity and ageostrophic velocity in the Ekman layer, and $p_s = p_s(x, y)$ is the surface pressure associated with large-scale circulation. The geostrophic velocity satisfies $\mathbf{u}_g = -\mathbf{k} \times \nabla p_s/\rho_w$, where $\mathbf{k}$ is the unit vector in the vertical direction. The corresponding boundary conditions are

$$Au_{e,z}|_{z=0} = \tau^x/\rho_w \quad \text{and} \quad Av_{e,z}|_{z=0} = \tau^y/\rho_w;$$
$$u_e, v_e \rightarrow 0, \qquad \text{at } z \rightarrow -\infty,$$

where the low limit should be interpreted as the base of the Ekman layer, and within the Ekman layer the vertical shear of the geostrophic velocity is negligible.

Multiplying these two equations by u^* and v^* and integrating the result over the depth of the Ekman layer leads to

$$E_t = S - P - D, \quad (9)$$

where

$$E = \rho_w \int_{-\infty}^{0} 0.5(u^{*2} + v^{*2}) \, dz,$$
$$S = \tau^x[u_g + u_e(0)] + \tau^y[v_g + v_e(0)],$$
$$P = \mathbf{U}_e \cdot \nabla p_s/\rho_w, \quad \text{and}$$
$$D = \rho_w \int_{-\infty}^{0} A(u_{e,z}^2 + v_{e,z}^2) \, dz$$

are the total kinetic energy of the Ekman layer, the rate of wind energy input, the rate of pressure work by the current integrated over the Ekman layer, and the rate of dissipation integrated over the Ekman layer, respectively. Note that the geostrophic velocity makes no contribution to pressure work because it is perpendicular to the pressure gradient. There is a simple relation:

$$P = \mathbf{U}_e \cdot \nabla p_s/\rho_w = \boldsymbol{\tau} \cdot \mathbf{u}_g; \quad (10)$$

that is, pressure work done by the Ekman transport is exactly the same as the wind stress work on the surface geostrophic currents. Thus, the right-hand side of Eq. (9) is reduced to the right-hand side of Eq. (5). The pressure work done by the Ekman transport is also related to the GPE generated by Ekman pumping:

$$\iint_S P \, dx \, dy = \iint_S \mathbf{U}_e \cdot \boldsymbol{\nabla} p_s / \rho_w \, dx \, dy$$

$$= -\iint_S w_e p_s / \rho_w \, dx \, dy + \oint \frac{p_s}{\rho_w} \mathbf{U}_e \cdot \mathbf{n} \, dl,$$
(11)

where S is the area of the ocean and $\mathbf{n}$ is the unit vector normal to the direction of integration l.

Equations (11) and (10) state that wind stress works on the surface geostrophic currents and is equal to the increase of GPE in the World Ocean from Ekman pumping, including coastal upwelling/downwelling (Gill et al. 1974; Fofonoff 1980). On the other hand, wind stress energy input to the surface ageostrophic current is used to maintain the Ekman spiral through the vertical turbulent dissipation in the Ekman layer.

The velocity field in the upper ocean is complicated. Observations indicate that, for time scales longer than a few weeks, the velocity profile in the upper ocean has structure that is closer to the spiral shape as described by the classical theory of the Ekman layer (Price et al. 1987; Plueddemann and Weller 1999). On the other hand, for time scales of near-inertial motions, the velocity structure is best described by a slab model. Wind energy input through near-inertial motions has been discussed in terms of a slab model by D'Asaro (1985), Watanabe and Hibiya (2002), and Alford (2003).

Thus, we will calculate the wind energy input to the surface current, using a classical 1D model for subinertial periods.

b. The steady solution

Assuming the diffusivity is vertically constant, the classical Ekman spiral solution gives rise to the velocity at the sea surface:

$$\mathbf{U}_{0E} = \frac{\sqrt{2}\,\boldsymbol{\tau}}{\rho_w f D_E} e^{-i\pi/4},$$

where

$$D_E = \sqrt{\frac{2A}{f}}.$$
(12)

Thus, the wind stress energy input is

$$W = \tau^2 / \rho_w f D_E.$$
(13)

c. Time-dependent wind forcing

In the following analysis, we introduce the complex variables $q = u + iv$ and $\tau = \tau^x + i\tau^y$ and use the Fourier expansion

$$q = \sum_{-\infty}^{\infty} Q_n e^{i\omega_n t} \quad \text{and} \quad \tau = \sum_{-\infty}^{\infty} T_n e^{i\omega_n t},$$

where

$$\omega_n = 2\pi n/T.$$

From Eq. (3), the nth component of the momentum equation is

$$Q_{n,zz} - i\frac{f + \omega_n}{A} Q_n = 0.$$

The total amount of wind energy input is

$$W = \sum_{-\infty}^{\infty} \frac{1}{\rho_w D_E} \sqrt{\frac{1}{|f(f + \omega_n)|}} T_n^2.$$
(14)

It is clear that, for high-frequency wind stress, the contribution to the energy is modified by a factor of $\sqrt{|f/(f + \omega_n)|}$. Thus in the Northern Hemisphere, the contribution from high-frequency anticlockwise wind is reduced, while the contribution from the clockwise wind is enhanced. Note that $f < 0$ in the Southern Hemisphere, and so the contribution from anticlockwise (clockwise) wind is enhanced (reduced).

3. Wind energy input to the surface Ekman layer in the oceans

a. Choice of Ekman depth

Although the Ekman theory has been the backbone of modern dynamical oceanography, the Ekman spiral predicted by classical theory has not been exactly verified. For a steady wind stress, the velocity vector on sea surface from classical theory is 45° to the right of wind stress (in the Northern Hemisphere), and the velocity vector rotates in the form of a spiral in a vertical direction. On the other hand, observations indicate that the angle between surface wind stress and surface drift velocity vector is in the range between 5° and 20° (Cushman-Roisin 1994). Recent observations also indicate that the surface velocity lies at more than the predicted 45° to the right of the wind. More important, the observed current amplitude decreases at a faster rate than it turns to the right; that is, the observed velocity profiles in the Ekman layer seem "flat" (Chereskin and Price 2001).

Despite efforts to find solutions that fit the observations, all models within the framework of the classical laminar theory (with a diffusivity independent of time) fail to produce the observed flat spiral. Other important dynamic processes, such as buoyancy flux through the air–sea interface, stratification, diurnal cycle, or even Stokes drift, may have to be included to explain the observed structure of the Ekman layer (Price and Sundermeyer 1999). Such models are clearly beyond the scope of this study.

Because of complicated dynamic processes in the upper ocean, parameterization of turbulent dissipation in the upper ocean remains a great challenge. Observations indicate that, in a thin surface layer immediately below the sea surface, waves and turbulent activities are strong, and so dissipation is near constant or slightly increases
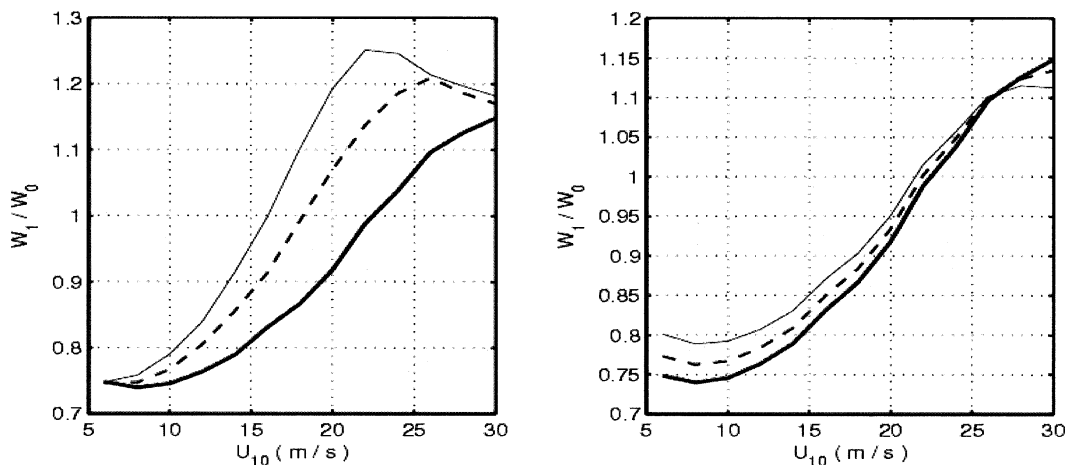
FIG. 1. Wind energy ratio R defined in Eq. (A12): (left) for different ratio of the interface height and roughness of the first layer: heavy line, $h = z_{01}$; dashed line, $h = 1.5z_{01}$; and thin line $h = 2.0z_{01}$ and (right) for different depth used in calculating the mean eddy viscosity: heavy line, $H = D_e$; dashed line, $H = 0.9D_e$; and thin line, $H = 0.8D_e$.

with depth; however, the dissipation rate declines with depth below this shallow layer. Direct observations in the California Current indicate that turbulent diffusivity declines exponentially for depth below 20 m (Chereskin 1995). Terray et al. (1996) carried out field observations and found that the dissipation rate is higher and roughly constant in a near-surface layer, but below this layer the dissipation rate decays as z^{-2}. This result is further refined as a -2.3 power law by Terray et al. (1999).

A crude model to represent this complexity is a two-layer model with a power law of vertical diffusivity in each layer (see the appendix). A simple linear profile $A = \alpha|z|$ was used in previous studies, for example, Madsen (1977). Such a profile is questionable because it is inconceivable that turbulent diffusivity is zero at the sea surface (Huang 1979). For the present case, we choose a linear profile for the surface layer, $n_1 = 1$, starting with a finite diffusivity on the sea surface. For the second layer, it is found that an inverse power profile with $n_2 = -0.7$ has a best fit for the diffusivity diagnosed by Chereskin (1995). The roughness and significant wave height can be estimated through an empirical relation $z_{01} = 0.85H_s$ (Terray et al. 1999), where H_s is significant wave height. For the case of long fetch, H_s can be estimated as $H_s = 0.30U^2/g$ (Wilson 1965), where U is wind speed and g is the gravitational acceleration; A_1 can be calculated as $A_1 = \kappa u_*$, where κ is von Kármán's constant and u_* is the friction velocity in the water (Craig and Banner 1994).

From this solution, the vertical diffusivity average A_m over a depth $H = cD_e$ (D_e is the e-folding depth of horizontal velocity) can be calculated and used in the classical model with a constant diffusivity. For typical cases, the work calculated from these two models is very close. Thus, in the following analysis, we will assume that vertical diffusivity is constant within the Ekman layer (Fig. 1).

There is no observational database for diffusivity A or the Ekman layer depth D_E. In this study, we choose an empirical formula:

$$D_E = \gamma \frac{u_{*w}}{f}, \qquad (15)$$

where $\gamma \approx 0.25$–0.4 is an empirical constant, determined from observations (Coleman et al. 1990; Price and Sundermeyer 1999). This relation implies that the equivalent vertical diffusivity at a given location is not a constant; instead, it depends on the wind stress and is inversely proportional to the Coriolis parameter. Using six sets of observations, including LOTUS-3 and LOTUS-4 (Long-Term Upper Ocean Study; Table 1 in Schudlich and Price 1998), SWAPP (Surface Waves Processes Program; Fig. 4a in Plueddemann and Weller 1999), Krauss (1993), Eastern Boundary Current (EBC), and 10°N (Fig. 11b in Price and Sundermeyer 1999), we found the best-fit value is $\gamma \approx 0.5$ (Fig. 2). Thus, energy input to the Ekman layer is

$$W = \frac{2}{\rho_w u_{*w}} \sum_{-\infty}^{\infty} \sqrt{\frac{1}{|(1 + \omega_n/f)|}} T_n^2, \qquad (16)$$

where u_{*w} is defined by the time-mean wind stress. From this formula, the energy input to the surface Ekman layer is roughly proportional to the third power of the frictional velocity, with a relatively minor dependency on the Coriolis parameter and frequency of the wind stress. It is also clear that, when $\omega \to -f$, resonance of the near-inertial motions can substantially boost the energy input, however, our focus in this study does not really cover this regime, as discussed above.

Note that Eq. (16) is based on the classical Ekman spiral, which predicts an angle of 45° to the right of the wind stress (Northern Hemisphere). As discussed above, field measurements indicate a much smaller angle in deviation; thus, using this formula we may underestimate the energy input.

b. Application to the World Ocean

The 1D model has been applied to the daily daily-mean wind stress data from the National Oceanic and Atmospheric Administration/National Centers for Environmental Prediction (NCEP)–National Center for Atmospheric Research (NCAR) from 1948 to 2002. These wind stress data have a zonally uniform spacing of 1.875° and a meridionally nonuniform spacing that varies from 1.89° at the Poles to 2.1° near the equator.

Using the complex-variable fast Fourier transform to the time series at each grid point, the cutoff frequency is $\omega = 0.5$ cycle day^{-1}. Thus, our calculation basically does not cover the energy input to near-inertial motions. Recent studies on wind energy input to near-inertial motions in the oceans give an estimate of 0.5–0.7 TW (Watanabe and Hibiya 2002; Alford 2003), and the calculation discussed here covers the contribution to a steady-state and subinertial frequency.

Wind energy input to the surface Ekman layer is very strong over three regimes (Fig. 3): 1) the Antarctic Circumpolar Current; 2) the South Indian Ocean, in particular; and 3) subpolar basins in the North Pacific and North Atlantic Oceans, which are coincident with the location of the storm track. On the other hand, this energy input is relatively weak along the equatorial band.

The total amount of energy from our calculation is 2.3 TW for the global oceans; see Table 1. Note that energy input to the Southern Hemisphere is 80% larger than to the Northern Hemisphere, probably because of strong currents driven by wind stress over the Southern Ocean, especially the Antarctic Circumpolar Current. The input through the steady component of wind stress

in the Southern Hemisphere (0.4 TW) is much larger than in the Northern Hemisphere (0.14 TW), which is probably due to the strong steady wind stress over the Southern Ocean.

As a comparison, we also performed a calculation based on the assumption of a constant depth of the Ekman spiral, $D_E = 50$ m. Note that under such an assumption energy input would be proportional to the fourth power of friction velocity instead of the third power implied in Eq. (16). The total amount of energy and its distribution in the space and frequency domains change accordingly. The global sum of energy input coincidently remains almost the same, 2.27 TW. However, the spatial distribution is different; there would be a peak of energy input near the equator, which may not be realistic (figure not shown).

In the Northern Hemisphere, energy input by the clockwise rotating wind stress is 0.39 TW, which is slightly larger than that from the anticlockwise rotating wind stress (0.3 TW); see Table 1. In the Southern Hemisphere, energy input by the anticlockwise rotating wind stress is 0.60 TW, which is much larger than that from the clockwise rotating wind stress (0.44 TW). The difference in energy inputs from clockwise and anticlockwise wind stress is, at least partially, due to the factor of $1 + \omega_n/f$ in the denominator of Eq. (16).

There are several peaks in the energy power spectrum, which correspond to periods of 1, 1/2, and 1/3 yr (Fig. 4). The most interesting phenomenon is the maximum in energy flux at the annual frequency along the coast of Somalia, which is closely related to the reverse of the Somali Jet, and in the western boundary of the subtropical gyre of the North Pacific. Such spatial patterns of wind energy input may have important implications for mixed layer dynamics at these locations (Fig. 5).

Wind energy input to the surface Ekman layer varies greatly from year to year (Fig. 6). Over the past 54 yr, the total energy input has increased from 2.1 to 2.4 TW, and this change is clearly related to the increase of wind stress over the same period of time. The increase of wind stress over the past 50 yr may be partially related to the improvement of instrumentation. In addition, climate change may also contribute. However, the exact nature of such a long-term trend in wind stress is beyond the scope of this study. For the period of 1997–2002, the mean energy input rate is 2.43 TW.

4. Conclusions

Using a combination of a simple analytical formula for the Ekman spiral and an empirical formula for the Ekman depth, we have calculated the energy input through the surface ageostrophic current from the Ekman spiral. For the period of 1997–2002, the rate of energy input for the subinertial frequency range is estimated as 2.4 TW; thus, in addition to the near-inertial wave contribution of 0.5–0.7 TW calculated by Alford
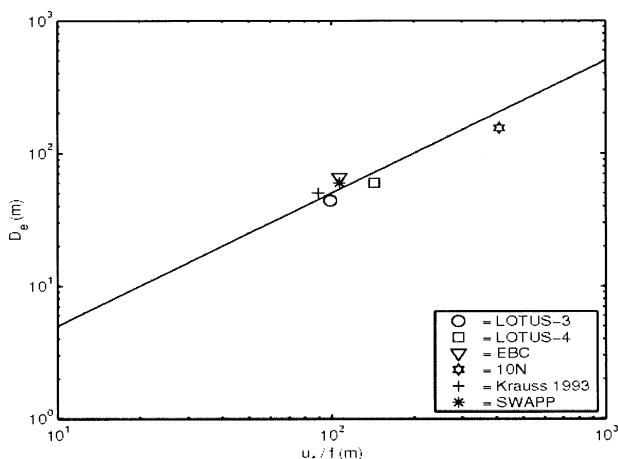

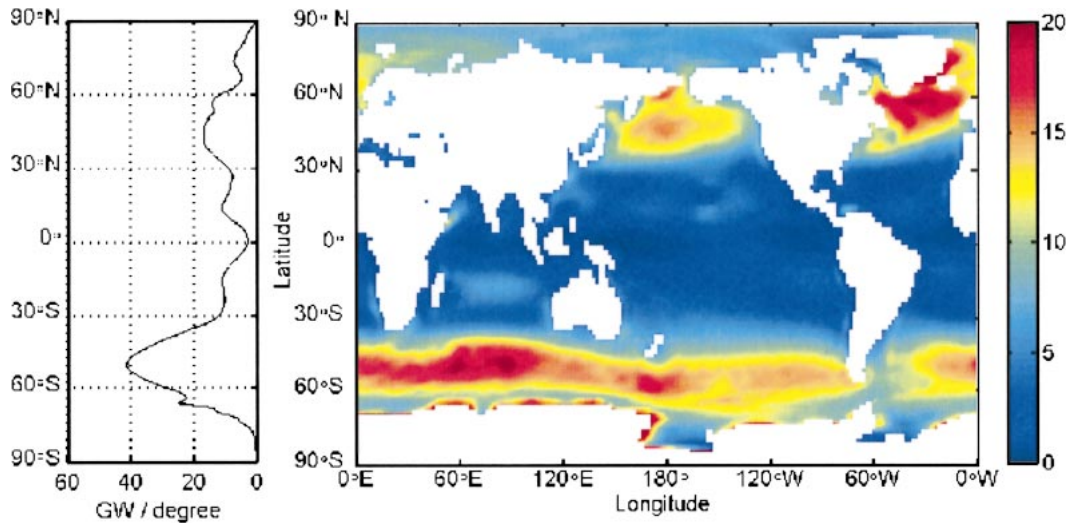FIG. 2. The relation between the Ekman depth D_e and u_{*w}/f.

FIG. 3. Distribution of the total wind energy input to the surface Ekman layer (mW m^{-2}) cut off at a frequency of 0.5 cycle day^{-1}.

(2003) and Watanabe and Hibiya (2002), the total energy input to the Ekman layer is estimated as 3 TW.

Energy input through the subinertial range is likely to be spent on supporting turbulence and mixing in the Ekman layer and thus maintains the velocity and stratification field in the upper ocean. This is an important part of the oceanic general circulation, although this energy input does not seem to contribute to the large-scale circulation directly. However, there might be interaction between the Ekman layer and fluids below, so that some part of this energy may be used to support turbulence and mixing below the Ekman layer; however, the details of these interactions remain unclear at this time.

On the other hand, wind stress energy input to the surface geostrophic current, estimated as 1.3 TW by Wunsch (1998), is mostly converted into the GPE through Ekman pumping. However, there is an intimate interplay between the geostrophic and ageostrophic components of the velocity in the upper ocean. Thus, energy input through the geostrophic currents and ageostrophic currents shows the currents are closely related to each other.

Our estimate should be interpreted with caution. First, our calculation is based on the classical spiral, assuming a constant viscosity. It is well known that circulation and water mass properties in the upper ocean can also

be described in terms of a slab model, especially for a time scale comparable with the inertial period. The choice of a spiral model used in our calculation is, of course, an idealization. Further study is needed to explore this separation in the frequency domain more carefully.

Second, choice of the Ekman layer depth is primarily based on an empirical formula. Although the case with a constant Ekman depth was also briefly discussed, a close examination on the effect of Ekman layer depth is needed.

Third, many complicated processes have been omitted in this discussion, such as the effect of stratification, surface waves, and heat and freshwater fluxes through
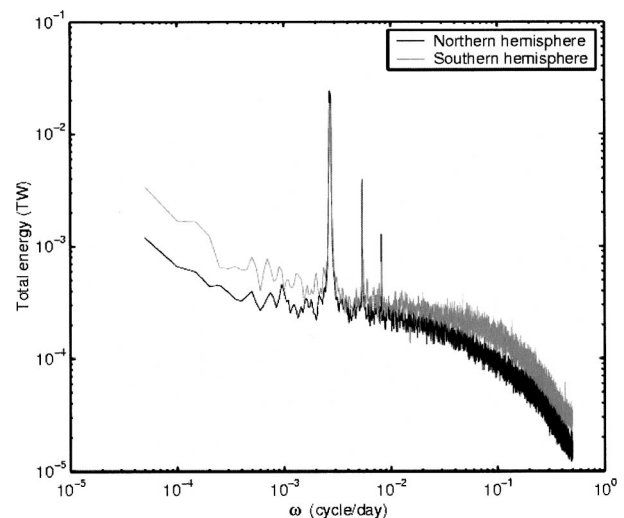
TABLE 1. Distribution of the wind energy input to the surface Ekman layer (TW), with cutoff frequency at $\omega = 0.5$ cycle day^{-1}.

	$\omega > 0$	$\omega < 0$	$\omega = 0$	Sum
Northern Hemisphere	0.30	0.39	0.14	0.83
Southern Hemisphere	0.60	0.44	0.40	1.44
Total	0.90	0.83	0.54	2.27

FIG. 4. Surface Ekman layer energy spectrum from wind stress for the Northern (black line) and Southern (gray line) Hemispheres.
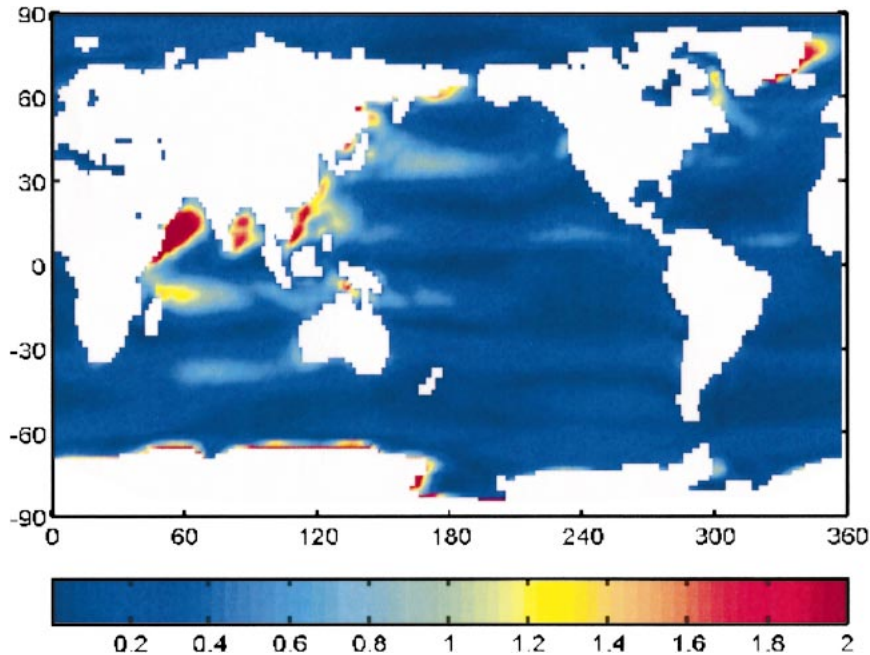
FIG. 5. Distribution of the total wind energy input to the surface Ekman layer (mW m^{-2}), at frequency of 1 cycle yr^{-1}.

the air–sea interface. Including these processes will make the calculations more accurate and meaningful.

Last, we emphasize the approximate nature of our calculation. All numbers presented in this study are offered with some uncertainty. It is anticipated that these calculations will serve as a first step toward understanding the energy input through the Ekman layer and its dynamical consequence.
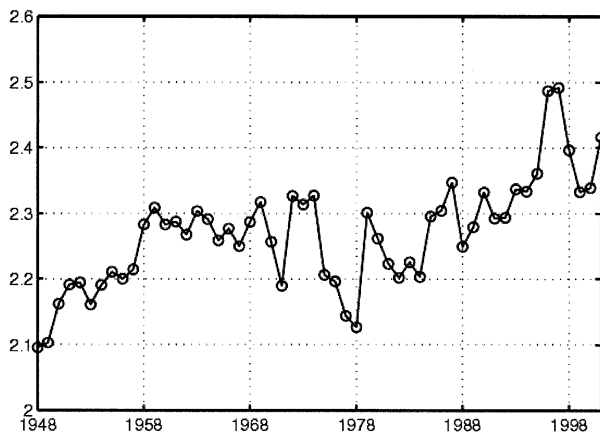
FIG. 6. Changes of the wind energy input to the Ekman layer for the global oceans over the past 54 yr.

APPENDIX

Ekman Spiral of a Two-Layer Model

The vertical eddy viscosity of a two-layer model is

$$A = \begin{cases} A_1(z_{01} - z)^{n_1} & \text{at } z \geq -h \\ A_2[z_{02} - (z + h)]^{n_2} & \text{at } z \leq -h, \end{cases} \quad (A1)$$

where $A_2 = A_1(z_{01} + h)\int^{n_1}$ and n_1 and n_2 are arbitrary real numbers; z_{01} and z_{02} are roughnesses at the surface and interface, respectively. Through straightforward but tedious algebraic manipulation, the horizontal velocity of the Ekman spiral is as follows:

$$w_1 = u_1 + iv_1 = B_1 s_1^{b_1}[c_1 J_{b_1}(s_1) + c_2 Y_{b_1}(s_1)]$$
$$\text{as } z \geq -h$$
$$w_2 = u_2 + iv_2 = c_3 s_2^{b_2}[J_{b_2}(s_2) - iY_{b_2}(s_2)]$$
$$\text{as } z \leq -h, \quad (A2)$$

where subscripts 1 and 2 represent the upper and lower layers, $J_b(s)$ and $Y_b(s)$ are the bth-order Bessel functions of the first and second kind,

$$b_1 = \frac{1 - n_1}{2 - n_1}, \qquad\qquad b_2 = \frac{1 - n_2}{2 - n_2}, \tag{A3}$$

$$s_1 = s_{01}\left(1 - \frac{z}{z_{01}}\right)^{(2-n_1)/2}, \qquad s_{01} = \frac{\sqrt{2E_1}}{2 - n_1}(1 - i), \qquad E_1 = \frac{fz_{01}^2}{A_1}, \tag{A4}$$

$$s_2 = s_{02}\left(1 - \frac{z + h}{z_{02}}\right)^{(2-n_2)/2}, \qquad s_{02} = \frac{\sqrt{2E_2}}{2 - n_2}(1 - i), \qquad E_2 = \frac{fz_{02}^2}{A_2}, \tag{A5}$$

$$c_1 = -\frac{Y_{b_1-1}(s_{1h}) - B_2 Y_{b_1}(s_{1h})}{Y_{b_1}(s_{01})[J_{b_1-1}(s_{1h}) - B_2 J_{b_1}(s_{1h})] - J_{b_1-1}(s_{01})[Y_{b_1-1}(s_{1h}) - B_2 Y_{b_1}(s_{1h})]}, \tag{A6}$$

$$c_2 = \frac{J_{b_1-1}(s_{1h}) - B_2 J_{b_1}(s_{1h})}{Y_{b_1}(s_{01})[J_{b_1-1}(s_{1h}) - B_2 J_{b_1}(s_{1h})] - J_{b_1-1}(s_{01})[Y_{b_1-1}(s_{1h}) - B_2 Y_{b_1}(s_{1h})]}, \tag{A7}$$

$$c_3 = \frac{s_{01}^{b_1}}{s_{02}^{b_2}}\left(1 + \frac{h}{z_{01}}\right)^{(1-n_1)/2}\frac{c_1 J_{b_1}(s_{1h}) + c_2 Y_{b_1}(s_{1h})}{J_{b_2}(s_{02}) - iY_{b_2}(s_{02})}, \tag{A8}$$

$$B_1 = -\frac{\tau^x + i\tau^y}{\sqrt{2A_1 f}\,\rho_0}\frac{1 + i}{s_{01}^{b_1}}, \quad \text{and} \tag{A9}$$

$$B_2 = \frac{(2 - n_2)z_{01}s_{02}}{(2 - n_1)z_{02}s_{01}}\left(1 + \frac{h}{z_{01}}\right)^{n_1/2}\frac{J_{b_2-1}(s_{2h}) - iY_{b_2-1}(s_{2h})}{J_{b_2}(s_{2h}) - iY_{b_2}(s_{2h})}, \tag{A10}$$

with $s_{jh} = s_j(h)$, $j = 1, 2$. The wind energy input to the Ekman spiral is

$$W_1 = \tau^x u + \tau^y v$$

$$= \frac{\tau^{x^2} + \tau^{y^2}}{\sqrt{2A_1 f}\,\rho_0}\operatorname{Re}\left\{-s_{01}^{b_1}[c_1 J_{b_1}(s_{01}) + c_2 Y_{b_1}(s_{01})]\frac{1 + i}{s_{01}^{b_1}}\right\}. \tag{A11}$$

As compared with the energy flux based on a classical Ekman solution with a constant diffusivity A_m, the ratio is

$$R = \frac{W_1}{W_0}$$

$$= \sqrt{\frac{A_m}{A_1}}\operatorname{Re}\left\{-s_{01}^{b_1}[c_1 J_{b_1}(s_{01}) + c_2 Y_{b_1}(s_{01})]\frac{1 + i}{s_{01}^{b_1}}\right\}. \tag{A12}$$

REFERENCES

Alford, M. H., 2003: Improved global maps and 54-year history of wind-work on ocean inertial motions. *Geophys. Res. Lett.,* **30,** 1424, doi:10.1029/2002GL016614.

Chereskin, T. K., 1995: Direct evidence for an Ekman balance in the California Current. *J. Geophys. Res.,* **100,** 18 261–18 269.

——, and J. F. Price, 2001: Ekman transport and pumping. *Encyclopedia of Ocean Sciences,* J. H. Steele et al., Eds., Academic Press, 809–815.

Coleman, G. N., J. H. Ferziger, and P. R. Spalart, 1990: A numerical study of the turbulent Ekman layer. *J. Fluid Mech.,* **213,** 313–348.

Craig, P. D., and M. L. Banner, 1994: Modeling wave-enhanced turbulence in the ocean surface layer. *J. Phys. Oceanogr.,* **24,** 2546–2559.

Cushman-Roisin, B., 1994: *Introduction to Geophysical Fluid Dynamics.* Prentice Hall, 320 pp.

D'Asaro, E. A., 1985: The energy flux from the wind to near-inertial motions in the surface mixed layer. *J. Phys. Oceanogr.,* **15,** 1043–1059.

Faller, A., 1966: Sources of energy for the ocean circulation and a theory of the mixed layer. *Proc. Fifth U.S. National Congress of Applied Mechanics,* Minneapolis, MN, ASME, 651–672.

Fofonoff, N. P., 1980: The Gulf Stream system. *Evolution of Physical Oceanography,* B. A. Warren and C. Wunsch, Eds., The MIT Press, 112–139.

Gill, A. E., J. S. A. Green, and A. J. Simmons, 1974: Energy partition in the large-scale ocean circulation and the production of mid-ocean eddies. *Deep-Sea Res.,* **21,** 499–528.

Huang, N. E., 1979: On surface drift currents in the ocean. *J. Fluid Mech.,* **91,** 191–208.

Huang, R. X., 1998: On the balance of energy in the oceanic general circulation. *Chin. J. Atmos. Sci.,* **22,** 452–467.

——, 1999: Mixing and energetics of the thermohaline circulation. *J. Phys. Oceanogr.,* **29,** 727–746.

——, 2002: Corrigendum. *J. Phys. Oceanogr.,* **32,** 1593.

Krauss, W., 1993: Ekman drift in homogeneous water. *J. Geophys. Res.,* **98,** 20 187–20 209.

Lueck, R., and R. Reid, 1984: On the production and dissipation of mechanical energy in the ocean. *J. Geophys. Res.,* **89,** 3439–3445.

Madsen, O. S., 1977: A realistic model of the wind-induced Ekman boundary layer. *J. Phys. Oceanogr.,* **7,** 248–255.

Munk, W. H., and C. Wunsch, 1998: The moon and mixing: Abyssal recipes II. *Deep-Sea Res.,* **45A,** 1977–2010.

Plueddemann, A., and R. A. Weller, 1999: Structure and evolution of the ocean surface boundary layer during the Surface Waves Processes Program. *J. Mar. Syst.,* **21,** 85–102.

Price, J., and M. A. Sundermeyer, 1999: Stratified Ekman layers. *J. Geophys. Res.,* **104,** 20 467–20 494.

——, R. A. Weller, and R. R. Schudlich, 1987: Wind-driven ocean currents and Ekman transport. *Science,* **238,** 1534–1538.

Sandstrom, J. W., 1916: Meteorologische studien im schwedischen Hochgebirge (Meteorological studies in the Swedish high mountains). *Goteborgs K. Vetensk. Vitterheis-Samh. Handl. Ser. 4,* **22,** 1–48.

Schudlich, R. R., and J. Price, 1998: Observations of seasonal variation in the Ekman layer. *J. Phys. Oceanogr.,* **28,** 1187–1204.

Terray, E. A., M. A. Donelan, Y. A. Agrawal, W. M. Drennan, K. K. Kahma, A. J. Williams III, P. A. Hwang, and S. A. Kitaigorodskii, 1996: Estimates of kinetic energy dissipation under breaking waves. *J. Phys. Oceanogr.,* **26,** 792–807.

——, W. M. Drennan, and M. A. Donelan, 1999: The vertical structure of shear and dissipation in the ocean surface layer. *The Wind-Driven Air–Sea Interface,* M. L. Banner, Ed., School of Mathematics, University of New South Wales, 239–245.

Wang, W., and R. X. Huang, 2004: Wind energy input to the surface waves. *J. Phys. Oceanogr.,* **34,** 1276–1280.

Watanabe, M., and T. Hibiya, 2002: Global estimates of the wind-induced energy flux to inertial motion in the surface mixed layer. *Geophys. Res. Lett.,* **29,** 1239, doi:10.1029/2001GL04422.

Wilson, B. W., 1965: Numerical prediction of ocean waves in the North Atlantic for December, 1959. *Dtsch. Hydrogr. Z.,* **18,** 114–130.

Wunsch, C., 1998: The work done by the wind on the oceanic general circulation. *J. Phys. Oceanogr.,* **28,** 2332–2340.